Materials Research. 2019; 22(6): e20190005
DOI: http://dx.doi.org/10.1590/1980-5373-MR-2019-0005

Morphology, Crystalline Structure and Chemical Composition Of MAO Treated Ti-15Zr-Mo Surfaces Enriched with Bioactive Ions

***Tiago Santos Pereira Sousa*[a]*, *Natália de Araujo da Costa*[a], *Diego Rafael Nespeque Correa*[a,b,c], *Luis Augusto Rocha*[a], *Carlos Roberto Grandini*[a,b]**

[a]*Instituto de Biomateriais, Tribocorrosão e Nanomedicina, Universidade Estadual Paulista (UNESP), CEP 17033-360, Bauru, SP, Brasil*
[b]*Laboratório de Anelasticidade e Biomateriais, Universidade Estadual Paulista (UNESP), CEP 17033-360, Bauru SP, Brasil*
[c]*Instituto Federal de Educação, Ciência e Tecnologia de São Paulo (IFSP), Grupo de Pesquisa em Materiais Metálicos Avançados, CEP 18095-410, Sorocaba, SP, Brasil*

Received: January 03, 2019; Revised: September 03, 2019; Accepted: 0ctober 24, 2019

In this study, MAO treatment was used to enrich, with bioactive Ca, Mg and P atoms, as-casted and heat-treated Ti-15Zr-xMo (x = 0, 5, 10 and 15 wt%) alloys, for potential use as advanced metallic biomaterials. The chemical composition of the surface was evaluated by EDS and XPS measurements. The morphology and microstructure was analyzed by OM and SEM images. Crystalline structure and phase composition were characterized by XRD measurements. The results indicated that the oxide layers were porous, with microstructural features of the bulk (grain size and secondary phases) slightly affecting the surface characteristics (pore size, chemical and phase composition). The crystalline structure of the oxide layers were composed by a mixture of anatase and rutile phases (TiO_2), with a minority of tetragonal zirconia (ZrO_2) and traces of $CaCO_3$ and P_2O_3 compounds. Chemical analysis indicated that the oxide layers were composed mainly by Ti and Zr oxides, with successful incorporation of the bioactive elements. The obtained results evidenced that the surface characteristics of MAO-treated Ti surfaces can be properly adjusted by the addition of alloying elements and implementation of specific heat treatments on the substrate. This finding can be quite useful for the development of novel biomedical implants.

Keywords: *biomaterial; Ti alloy; micro-arc oxidation; oxide layer; bioactivity.*

1. Introduction

In the manufacturing of metallic biomaterials, titanium (Ti) and its alloys are the best choice, due their optimal combination of high strength-to-density ratio, excellent corrosion resistance, relatively low Young's modulus when compared to other commercial alloys (e.g. SS316L and CoCrMo alloys), and recognized biocompatibility[1]. With the aim to reduce the long-term failures of the implant, caused mainly by stress shielding effect, it has been sought β-type Ti alloys, with Young's modulus closer than the human bones[2]. In this scenery, Ti-15Zr-xMo alloys have been recently investigated as a viable alternative for the processing of novel load-bearing implants[3]. Molybdenum (Mo) is known as a strong β-stabilizer alloying element, acting as a solution solid hardener and in the increasement of the corrosion resistance and mechanical strength, when added to Ti-based alloys[4,5]. Zirconium (Zr) is a neutral element, but in the presence of Mo promotes a slightly β-stabilizer action. As an alloying element, it can decrease the melting point of the solid solution, improve the mechanical strength and enhance the biocompatibility[6,7].

In an earlier study, Correa et al.[8] showed that the addition of Mo on Ti-15Zr-based alloy led to a noticeable decreasement of the Young's modulus, having the Ti-15Zr-15Mo (wt%) alloy displayed the best combination of mechanical properties for potential use as metallic biomaterials. However, for a successful employment as a biomedical implant, it is crucial a friendly surface, once it will be in close contact with the biological host[2]. In this sense, surface modification techniques have been constantly applied to Ti surfaces. Among them, micro-arc oxidation (MAO) technique has received special attention, once it is a fast, versatile and low-cost method for surface modification[9,10]. In this technique, it is possible to control the electrochemical parameters involved, such as electrolyte's composition, applied potential and current, time and temperature, which results in thick porous oxide layers, strongly bound to the substrate[11].

Setting up the electrolyte's composition properly, it is possible to incorporate some elements into the oxide layers, which can affect its biocompatibility, bioactivity and osseointegrative capability. Calcium (Ca), phosphorus (P) and magnesium (Mg) are the main choices to build biomultifunctional surfaces, once they are the main constituents of the human bones, which turns possible to fast bone regeneration and growth[10]. Smika et al.[12] performed MAO-treatment in the

*Corresponding author: tiagospsousa@hotmail.com

biomedical β-type Ti-15Mo alloy, enriching the oxide layer with Ca and P atoms. The results indicated a significant increasement of the corrosion resistance of the material after surface modification. Tsai et al.[13] fabricated MAO-treated surfaces on α-type Ti-Zr films, which were previously deposited over CP-Ti by sputtering. The results indicated that the porous and multicomponent oxide layers produced an enhanced biological performance when in contact with human osteosarcoma cells and skin fibroblasts, evidencing its high potential for biomedical use. In a previous study, Correa et al.[14] found that MAO-treated surfaces, enriched with Ca and P, grown on Ti-15Zr-xMo alloys are biocompatible and bioactive. However, it was not evaluated the effect of Mg element into the oxide layers, as well as the substrate's phase composition and microstructure. As observed by Oliveira et al.[9], the presence of Mg, into the oxide layers of MAO-treated CP-Ti surface, can have a positive impact on the surface mechanical properties, tribocorrosion and corrosion resistances, and also improve its bioactivity and biocompatibility.

Take it into account, the main purpose of this study was to investigate the surface characteristics of the oxide layer grown on Ti-15Zr-xMo (0, 5 and 15 wt%) alloys, treated by MAO and enriched with Ca, P and Mg atoms. The crystalline structure and microstructure were altered by the alloying elements and a homogenization heat treatment, and the produced oxides layers were analyzed regarding morphology, composition and crystalline structure.

2. Materials and Methods

For the manufacture of the Ti-15Zr-xMo (x = 0, 5 and 15 wt%) samples, commercially pure metals were used as raw materials: CP-Ti (grade 2), pure Zr (99.8%) and pure Mo (99.9%). The metals were separated on their respective quantities for each sample, immersed in an etching solution (HNO_3 and HF), for around 15 s, and washed in an ultrasonic bath with acetone for 600 s. The samples were obtained by argon arc-melting, with a water-cooled copper crucible and non-consumable tungsten electrode. The ingots were remelted for 5 times to ensure a complete mixture of the alloying elements. After that, the ingots were subjected to a homogenization heat treatment, a vacuum of 10^{-7} Torr, in 1173 K, during 14.4 ks, and heating/cooling rate of around 0.08 K/s. Then, the samples were sectioned by a diamond cutting wheel, resulting in lamellar pieces with thickness of around 1 mm. Finally, the cleaning process was repeated, composed by the same etching process (with HNO_3 and HF solution) and ultrasonic bath, but now in isopropyl alcohol (600 s) and distilled water (300 s).

The MAO treatments were carried out in a DC power source (Keysight, N5751A model) operating at 300 V, with limited current of 2.5 A, for 60 s. The surface modifications were perfomed at room temperature (~ 300 K), being constantly monitored by a digital thermometer. The samples were set up as a positive electrode (anode) and a platinum plate as a counter-electrode (cathode). The distance between the electrodes remained around 80 mm in all treatments. The electrolyte was composed by 0.35 M calcium acetate monohydrate ($C_4H_6CaO_4.H_2O$), 0.02 M β-glycerol phosphate ($C_3H_7Na_2O_6P.5H_2O$) and 0.10 M magnesium acetate tetrahydrate ($C_4H_6MgO_4.4H_2O$). The electrolyte was constantly mixed during the surface treatment. The samples were posteriorly cleaned with distilled water, dried in air stream, and kept in a dessicator.

Chemical analysis of the bulk and surface regions was carried out by X-ray energy dispersive spectroscopy (EDS, Oxford, Inca model) and X-ray photoelectron spectroscopy (XPS, Thermo Scientific Spectra Inc., Thermo K-Alpha model), operating with monochromatic AlK_α radiation (1486 eV). The morphological and microstructural features were analyzed by scanning electron microscopy (SEM, Carl Zeiss microscope, LS15 EVO model) and optical microscopy (OM, Olympus microscope, model BX51M). The micrographs were lately evaluated by digital image analysis (ImageJ software). Before microstructural analysis, the samples were submitted to polishing with waterproof papers, until mesh of #1500, and colloidal diamond and silica suspensions, with 1.0 and 0.25 μm, respectively. To reveal the microstructure, the mirror-like surfaces were immersed in a chemical solution of H_2O, HNO_3 and HF (85:10:5), for around 30 s. The crystalline structure was evaluated by X-ray diffractometry (XRD, Panalytical diffractometer, X' Pert Pro model), with monochromatic CuK_α radiation (0.1544 nm), operating at 40 kV and 40 mA, Ni filtered, fixed time mode, collecting time of 3.0 s and step-size of 0.03°. An initial mechanical assessment was performed by Vickers microhardness test (Shimadzu Inc., HMV-2 model), with load of 0.300 kgf (2.942 N) and dwell-time of 60 s. The microhardness values were acquired along the transversal and longitudinal regions of the samples.

3. Results and Discussions

3.1. Bulk characterization

In the Fig. 1 is exhibited the structural and microstructural evolution of the samples in terms of chemical composition and heat treatment. The as-cast Ti-15Zr sample showed only martensitic α' phase (hcp), in the form of needle-like plates. The as-cast Ti-15Zr-5Mo sample was composed by thin acicular martensitic α" phase (orthorhombic) precipitates permeated along the β phase (bcc) grains. And finally, the as-cast Ti-15Zr-15Mo sample displayed only equiaxed β phase grains, indicating a pronounced decreasement of the β-transus temperature by the alloying elements[8,15]. Regarding the heat-treated samples, it is possible to notice some significant differences when compared to the as-cast

ones. The heat-treated Ti-15Zr sample exhibited a lamellar microstructure, possibly due to the phase transformation α' → α occurred during the slow cooling from the high temperature. In the heat-treated Ti-15Zr-5Mo sample, there was an enlargement of the acicular precipitates to a lamellar-like appearance, likely due to the metastable to stable phase transformations α' → α and β → α. For the heat-treated Ti-15Zr-15Mo sample, there was just a visible rise of the β phase grains, without any phase transformation, perhaps due to the proximity of the β transus temperature with the room temperature. Nevertheless, Xavier et al.[15] and Correa et al.[16] identified some α phase precipitates in this alloy after long-time aging treatments, which indicates that its β transus temperature still remains above the room temperature. It is worth to mention that these metastable phases (α' and α") was also found on some preliminary study[3], where it was investigated the crystalline structure and microstructure of homogeneized Ti-15Zr-xMo (0, 2.5, 5, 7.5, 10, 12.5, 15 and 20 %wt) as possible candidates for biomedical applications. Vickers microhardness values of the samples, compared with some commercial metallic biomaterials, are shown in the Fig. 2. All samples presented values above CP-Ti and comparable to the Ti-6Al-4V, as a result of the combination of solid solution and phase precipitation hardening effects, in accord to previous studies[4,17]. This result highlights the high mechanical strength of the studied samples, making them potential candidates for use as biomedical implants.

3.2. Surface characterization

3.2.1. Electrochemical analysis

The bulk characterization indicated that the samples can be classified as monophasic α, biphasic α + β and metastable β-type, which is in close agreement with earlier studies[3,16,18]. Therefore, we perfomed the MAO treatment in order to verify the effect of the substrate's crystalline structure and microstructure on the oxide layer. From the current-time curves of the MAO treatments (Fig. 3), it is possible to observe two distinct steps (galvanostatic and potentiostatic stages). In the galvanostatic stage, the current was kept limited to 2.5 A, while the oxide layer began to grow and small arcs was formed. As the oxide thickness raised, the dielectric barrier became larger, requiring a higher voltage to remain the current constant. The potentiostatic stage started when the voltage of 300 V was reached, the current went down while high energetic arcs were formed along the surface samples. These electric arcs generated local increasement of pressure and temperature, influencing pore size and shape, thickness and crystallization of the oxide layers[9,19]. It is also possible to observe that the duration of the galvanostatic stage varied on each sample, having the as-cast samples longer values than the heat-treated ones. This feature should be evaluated in future studies, once it directly impacts the total electric energy received by the

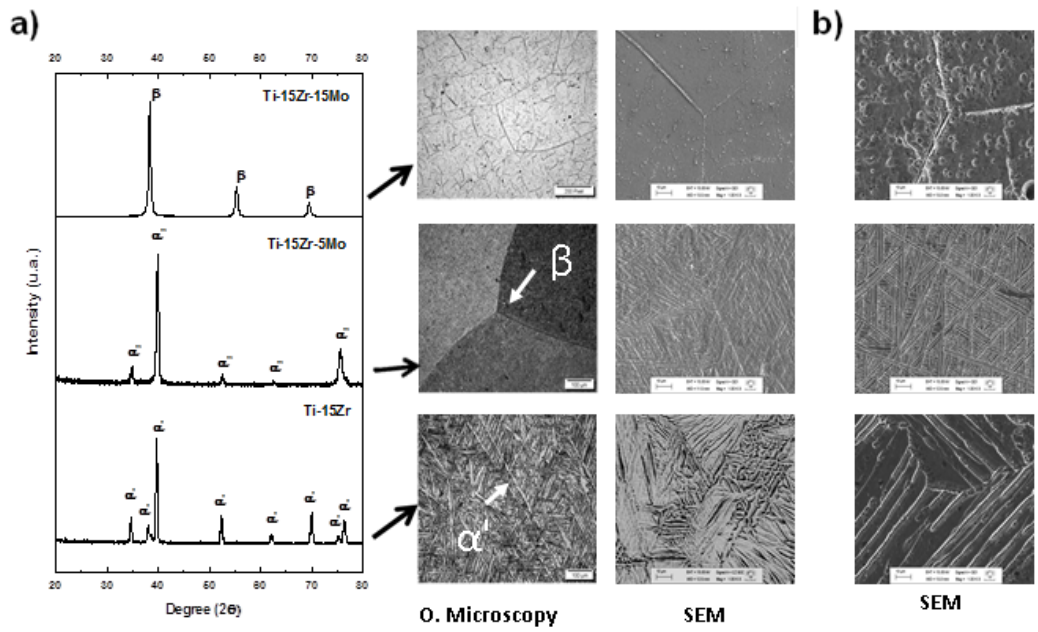

Figure 1: XRD patterns, OM and SEM images of Ti-15Zr-xMo samples in the a) as-cast and b) heat-treated conditions.

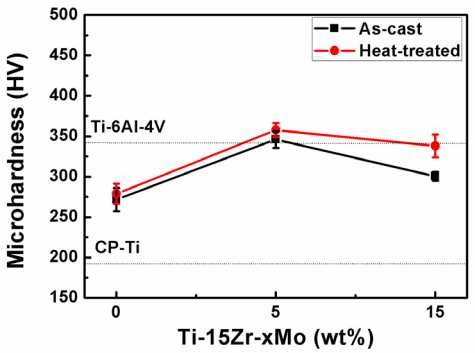

Figure 2: Vickers microhardness values.

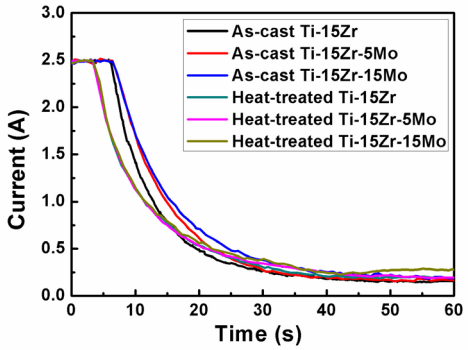

Figure 3: Current-time curves of the MAO treatments.

sample, affecting the surface characteristics and the amount of elements incorporated from the electrolyte, as pointed out by Oliveira et al.[9].

3.2.2. Morphological analysis

In the topographical images of the Fig. 4, it is noted that the oxide layers exhibited a typical porous morphology in all samples. These pores is characteristic of the MAO treatment, being a result of the dielectric breakdown of the oxide layer by the applied voltage[20]. The average pore distribution were measured for each sample, and the results are shown in Fig. 5. The as-cast Ti-15Zr sample had an average pore area of 1.12 μm^2, with a majority of pores (29%) in the range of 0.5 - 1.0 μm^2. In the heat-treated condition, the majority of the pores (36%) had an pore area lesser than 0.5 μm^2, with an average pore area of 1.08 μm^2. Similarily, the as-cast Ti-15Zr-5Mo sample had a decayment in the average pore area (0.94 μm^2), having the majority of pores (46%) placed between 0.5 - 1.0 μm^2. In the heat-treated condition, the average pore area and the majority of pores (33%) remained around 1.10 μm^2 and 0.5 - 1.0 μm^2, respectively. And finally, the as-cast Ti-15Zr-15Mo sample had an average pore area of 0.78 μm^2, with the majority of pores (37%) between 0.5 - 1 μm^2, whilst the heat-treated condition had the same average pore area, with a majority of the pores (43%) between 0.5 - 1 μm^2. In overall, the results suggest that the amount of Mo and heat treatment tended to decrease the pore size of the oxide layers. In addition, it is possible to note that the monophasic samples exhibited minor variation of the average pore area in relation to the biphasic one, which could be possible related to the distinct oxide layer growth mechanisms on the α and β phases. For example, Luz et al.[21] found differences in the oxidation of Ti atoms along the α and β phases on the Ti-10Nb alloy, when submitted to similar anodizing process. This finding supports our initial assumption that the microstructural features play a role on the surface oxide layer morphology of Ti surfaces after MAO treatment. Further cross-sectional analysis of the oxide layers can give more information about the pore and elemental distribuition, thickness and growth mechanisms[14].

3.2.3. Structural analysis

The XRD patterns of the MAO-treated samples are compared in the Fig. 6. First of all, it was possible to observe some diffracted peaks from the bulk in all samples (e.g. α', α" and β phases), which indicates that the oxide layer thicknesses were in order of micrometers. For the as-cast Ti-15Zr sample, the pattern was composed by a mixture of TiO_2 phases (anatase and rutile), with minor peaks of tetragonal zirconia (ZrO_2). The growth of rutile and tetragonal ZrO_2 phase in the oxide layers were a result of the local high temperature and pressure created by the electric arcs, which favored the precipitation of metastable or amorphous phases, as observed on previous studies[13,22]. It was not possible to observe any significant difference in the XRD pattern of the heat-treated sample. In the as-cast Ti-15Zr-5Mo sample, there was a similar phase composition of anatase, rutile and tetragonal zirconia oxides, but some diffracted peaks from Ca and P oxides were also clearly visible. The described peaks were related to $CaCO_3$ and P_2O_3 compounds, which indicates an abundance of incorporated bioactive atoms into the oxide layer. The XRD pattern of the heat-treated sample exhibited the same result when compared to the as-cast one. The XRD pattern of the as-cast Ti-15Zr-15Mo sample was quite similar to the as-cast Ti-15Zr-15Mo sample, with the exception of the abundance of amorphous phase on the heat-treated condition. Similar results were found by Correa et al.[14], whose identified nano-crystalline TiO_2 and ZrO_2 precipitates permeating a large amorphous layer on MAO-treated Ti-15Zr-xMo surfaces, when analyzed by TEM imaging. The broad halo observed on the XRD patterns of the Ti-15Zr-5Mo and Ti-15Zr-15Mo samples was related to the amorphous phase, which could be formed during the above-mentioned electric arcs generation. These results suggest that MAO-treated surfaces can have interesting properties from the biomedical point of view. The produced multicomponent oxide layer can be controlled by proper post heat treatments, which can produce a variety

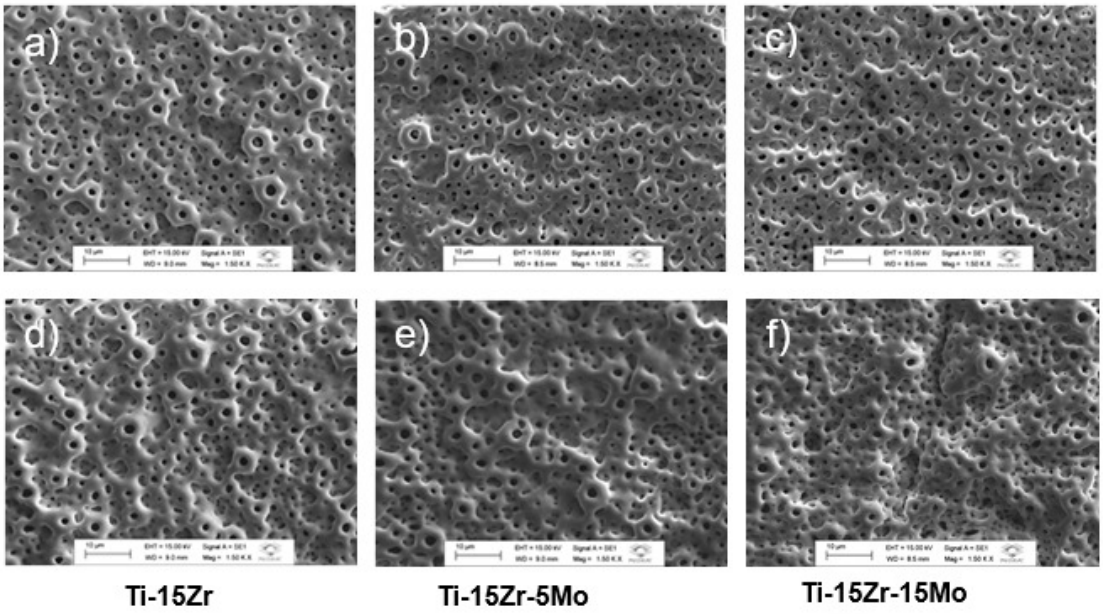

Figure 4: Morphology of the oxide layers obtained by MAO in the samples: as-cast (a, b and c) and heat-treated (c, d and f) conditions.

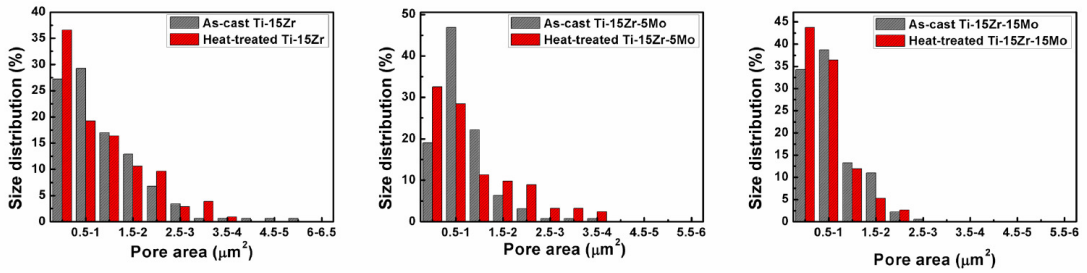

Figure 5: Normal distribution of the pore areas.

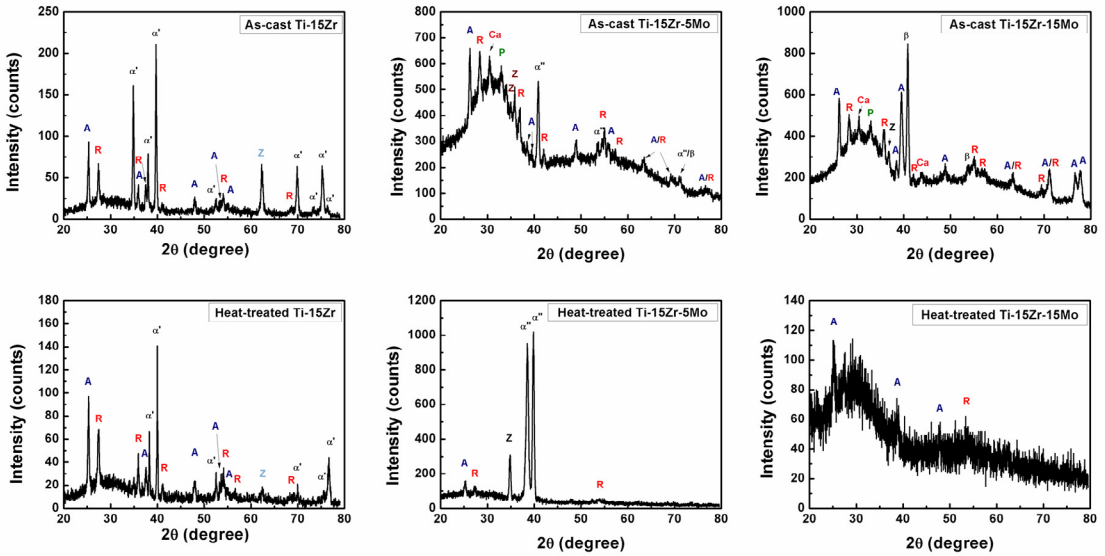

Figure 6: XRD patterns of MAO treated samples (A – anatase; R – rutile; Z – tetragonal zirconia; Ca – $CaCO_3$; P – P_2O_3).

of biological interactions with human cells and tissues, as observed on some studies[10,13,23].

3.2.4. Chemical analysis

A comparison between the EDS spectrums of the MAO-treated surfaces are shown in the Fig. 7. Ti-15Zr samples (as-cast and heat-treated conditions) exhibited peaks of Ti, Zr, Mo, Ca and Mg atoms, indicating that the bioactive elements were successfully incorporated into the oxide layers. Ti-15Zr-5Mo and Ti-15Zr-15Mo samples presented the same result, with the exception of the clear depletion of Mo peaks, in accord to the assumption that the oxide layers were formed preferentially by TiO_2 and ZrO_2[14]. The P atoms were not indexed, once its K_α energy (2.013 keV) is almost the same of the Zr's L_α energy (2.042 keV) in the EDS spectrum. A semi-quantitative EDS analysis of the incorporated bioactive elements as function of Mo is displayed in the Table 1. For all samples, the amount of Ca and Mg remained almost the same, being close to that found by Oliveira et al. in CP-Ti, after similar MAO treatment[9].

XPS results for the MAO-treated as-cast samples are exhibited in the Fig. 7, where it was detected all the alloying elements (Ti, Zr and Mo) together the bioactive elements (Ca, Mg and P). As the XPS' interaction volume is lesser than the EDS, it is possible to conclude that the outer region of the oxide layers were enriched with the bioactive elements. The high-resolution curves for the alloying and bioactive elements are shown in the Fig. 8. The Ti-2p curve was composed by the Ti-$2p_{3/2}$ and Ti-$2p_{1/2}$ doublet, with binding energy values around 458.5 eV and 464.3 eV for all samples. These high intense peaks indicate a majority of TiO_2 in the oxide layers, as expected by the high affinity of Ti with oxygen[24]. Similarly, the Zr-3d curve was composed by Zr-$3d_{5/2}$ and Zr-$3d_{3/2}$ doublet, with binding energy values close to 185.5 eV and 182.4 eV. In the same way, this result confirms the presence of a significant quantity of ZrO_2 in the oxide layers[13,24,25]. Regarding the Mo-3d curve, there was just sparse Mo-$3d_{3/2}$ and Mo-$3d_{5/2}$ doublet, with binding energy values near of 233.1 eV and 232.4 eV, possibly indicating a Mo-O type bounding. The low intensity of these peaks is an indicative of Mo depletion on the oxide layers[26]. The Ca-2p curve exhibited a Ca-$2p_{1/2}$ and Ca-$2p_{3/2}$ doublet, with binding energy values around 346.9 eV and 347.3 eV, which can be related to carbonates (e.g. $CaCO_3$)[27]. In the P-2p curve, there was just a P-$2p_{3/2}$ singlet, with binding energy values of 133.3 eV, likely as oxide (e.g. P_2O_3) or phosphate (e.g. $Ca_3(PO_4)_2$ or $Mg_3(PO_4)_2$) compounds[28,29]. Finally, for the Mg-1s curve, there was a singlet with binding energy values close to 1304.5 eV, which can indicate an oxide (MgO), carbonate ($MgCO_3$) or phosphate ($Mg_3(PO_4)_2$) bounding[30]. From the semi-quantitative XPS analysis of these elements depicted in the Table 2, it is possible to note that the amount of bioactive elements was not altered with the Mo content in the samples, indicating that the incorporation of elements

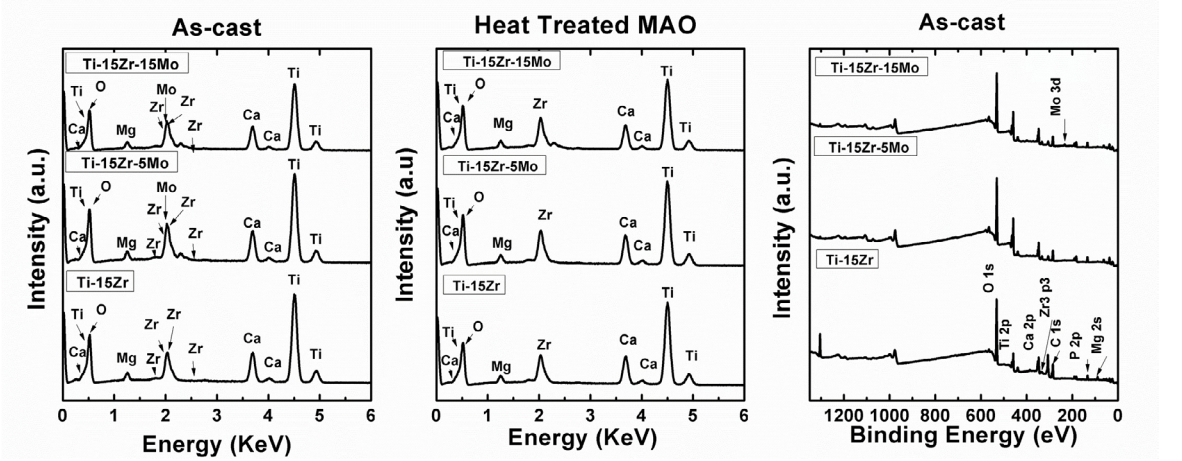

Figure 7: Chemical analysis: (a) EDS and (b) XPS spectra of the MAO-treated surfaces.

Table 1. Semi-quantitative EDS chemical composition of the bioactive elements.

Sample	Condition	Ca	Mg
Ti-15Zr	As-cast	7.9 ± 0.2	1.1 ± 0.2
	Heat-treated	8.4 ± 0.2	1.3 ± 0.2
Ti-15Zr-5Mo	As-cast	7.6 ± 0.2	1.1 ± 0.2
	Heat-treated	8.2 ± 0.2	1.3 ± 0.2
Ti-15Zr-15Mo	As-cast	7.5 ± 0.2	1.1 ± 0.2
	Heat-treated	7.9 ± 0.2	1.3 ± 0.2

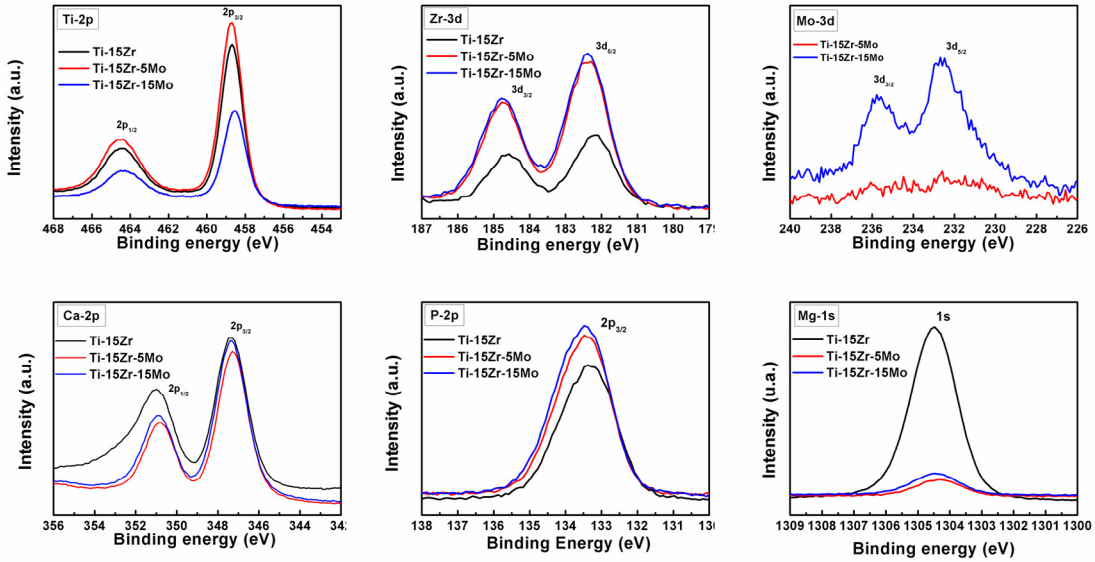

Figure 8: High resolution XPS spectra of the alloying and bioactive elements.

Table 2. Semi-quantitative XPS chemical composition of the bioactive elements.

As-cast samples	Ca	P	Mg
Ti-15Zr	10.63 ± 0.3	7.71 ± 0.3	5.59 ± 0.3
Ti-15Zr-5Mo	9.62 ± 0.3	8.9 ± 0.3	6.06 ± 0.3
Ti-15Zr-15Mo	9.42 ± 0.3	8.51 ± 0.3	5.49 ± 0.3

during MAO treatment was not affected by the substrate's chemical composition.

These results indicate that it is possible to produce porous oxide layers enriched with bioactive elements in the Ti-15Zr-xMo samples by using MAO treatment, likewise previous studies on CP-Ti's surfaces[9]. It was also noted that the surface oxide layer morphology can be adjusted by the chemical composition and microstructural features of the substrate. In this way, these MAO-treated samples can possess great potential to be applied as advanced biomedical implants, gathering mechanical biocompatibility, bioactivity and osseointegrative capabilities. Futher mechanical analyses, such as mechanical adhesion and tribological measurements can be performed in order to elucidate the advantages of these samples for the biomedical application.

4. Summary

The results reported in this paper give interesting findings about the effect of substrate on the MAO-treated surfaces. The amount of alloying elements affected the β-transus temperature of the samples, resulting in a monophasic α, biphasic α + β and entirely β phase microstructures. The heat treatment produced microstructural modifications in the substrate, favoring the appearance of secondary α phase from the metastable martensitic α' and α" phases. The MAO-treated surfaces exhibited a typical porous morphology, with similar pore area, which were composed by a mix of anatase and rutile phases (TiO_2), a minority of tetragonal zirconia (ZrO_2), and traces of $CaCO_3$ and P_2O_3 compounds. The bioactive elements were successfully incorporated into the oxide layers, having the alloying elements and heat treatment unchanged their quantities in the samples. These findings could be interesting for the development of novel biomedical implants, once they showed that a proper handling of the substrate's chemical composition and microstructure turned possible the controlling of the morphological features of MAO-treated surfaces.

5. Acknowledgments

The authors thank the Department of Physics from UNESP, Bauru (SP), for the SEM/EDS analysis. The National Nanotechnology Laboratory (LNNano) of the Research Center for Materials and Energy (CNPEM), Campinas (SP), for the XRD and XPS measurements. This study was financed by the Brazilian funding agencies: FAPESP (grant #2015/00851-6) and CNPQ (grant #134773/2016-0). The authors also acknowledge the reviewers, for their valuable comments.

6. References

1. Geetha M, Singh AK, Asokamani R, Gogia AK. Ti based biomaterials, the ultimate choice for orthopaedic implants - A review. *Progress in Materials Science*. 2009;54(3):397-425.

2. Prasad K, Bazaka O, Chua M, Rochford M, Fedrick L, Spoor J, et al. Metallic Biomaterials: Current Challenges and Opportunities. *Materials (Basel)*. 2017;10(8). pii: E884.

3. Correa DRN, Kuroda PAB, Lourenço ML, Fernandes CJC, Buzalaf MAR, Zambuzzi WF, et al. Development of Ti-15Zr-Mo alloys for applying as implantable biomedical devices. *Journal of Alloys and Compounds*. 2018;749:163-171.

4. Kuroda PAB, Buzalaf MAR, Grandini CR. Effect of molybdenum on structure, microstructure and mechanical properties of biomedical Ti-20Zr-Mo alloys. *Materials Science and Engineering: C*. 2016;67:511-515.

5. Cardoso FF, Ferrandini PL, Lopes ESN, Cremasco A, Caram R. Ti-Mo alloys employed as biomaterials: Effects of composition and aging treatment on microstructure and mechanical behavior. *Journal of the Mechanical Behavior of Biomedical Materials*. 2014;32:31-38.

6. Correa DRN, Vicente FB, Donato TAG, Arana-Chavez VE, Buzalaf MAR, Grandini CR. The effect of the solute on the structure, selected mechanical properties, and biocompatibility of Ti-Zr system alloys for dental applications. *Materials Science and Engineering: C*. 2014;34:354-359.

7. Cordeiro JM, Faverani LP, Grandini CR, Rangel EC, da Cruz NC, Nociti Junior FH, et al. Characterization of chemically treated Ti-Zr system alloys for dental implant application. *Materials Science and Engineering: C*. 2018;92:849-861.

8. Correa DRN, Vicente FB, Araújo RO, Lourenço ML, Kuroda PAB, Buzalaf MA, et al. Effect of the substitutional elements on the microstructure of the Ti-15Mo-Zr and Ti-15Zr-Mo systems alloys. *Journal of Materials Research and Technology*. 2015;4(2):180-185.

9. Oliveira FG, Ribeiro AL, Perez G, Archanjo BS, Gouvea CP, Araújo JR, et al. Understanding growth mechanisms and tribocorrosion behaviour of porous TiO_2 anodic films containing calcium, phosphorous and magnesium. *Applied Surface Science*. 2015;341:1-12.

10. Wang Y, Yu H, Chen C, Zhao Z. Review of the biocompatibility of micro-arc oxidation coated titanium alloys. *Materials & Design*. 2015;85:640-652.

11. Tian Y, Ding S, Peng H, Lu S, Wang G, Xia L, et al. Osteoblast growth behavior on porous-structure titanium surface. *Applied Surface Science*. 2012;261:25-30.

12. Simka W, Krząkała A, Korotin DM, Zhidkov IS, Kurmaev EZ, Cholakh SO, et al. Modification of a Ti–Mo alloy surface via plasma electrolytic oxidation in a solution containing calcium and phosphorus. *Electrochimica Acta*. 2013;96:180-190.

13. Tsai MT, Chang YY, Huang HL, Wu YH, Shieh TM. Micro-arc oxidation treatment enhanced the biological performance of human osteosarcoma cell line and human skin fibroblasts cultured on titanium-zirconium films. *Surface and Coatings Technology*. 2016;303(Pt A):268-276.

14. Correa DRN, Rocha LA, Ribeiro AR, Gemini-Piperni S, Archanjo BS, Achete CA, et al. Growth mechanisms of Ca- and P-rich MAO films in Ti-15Zr-xMo alloys for osseointegrative implants. *Surface and Coatings Technology*. 2018;344:373-382.

15. Xavier CC, Correa DRN, Grandini CR, Rocha LA. Low temperature heat treatments on Ti-15Zr-xMo alloys. *Journal of Alloys and Compounds*. 2017;727:246-253.

16. Correa DRN, Kuroda PAB, Lourenço ML, Buzalaf MAR, Mendoza ME, Archanjo BS, et al. Microstructure and selected mechanical properties of aged Ti-15Zr-based alloys for biomedical applications. *Materials Science and Engineering: C*. 2018;91:762-771.

17. Ho WF, Wu SC, Hsu SK, Li YC, Hsu HC. Effects of molybdenum content on the structure and mechanical properties of as-cast Ti–10Zr-based alloys for biomedical applications. *Materials Science and Engineering: C*. 2012;32(3):517-522.

18. Correa DRN, Kuroda PAB, Lourenço ML, Buzalaf MAR, Grandini CR. Adjustment of the microstructure and selected mechanical properties of biomedical Ti-15Zr-Mo alloys through oxygen doping. *Journal of Alloys and Compounds*. 2019;775:158-167.

19. Alves SA, Rossi AL, Ribeiro AL, Werckmann J, Celis JP, Rocha LA, et al. A first insight on the bio-functionalization mechanisms of TiO_2 nanotubes with calcium, phosphorous and zinc by reverse polarization anodization. *Surface and Coatings Technology*. 2017;324:153-166.

20. Alves AC, Oliveira F, Wenger F, Ponthiaux P, Celis JP, Rocha LA. Tribocorrosion behaviour of anodic treated titanium surfaces intended for dental implants. *Journal of Physics D: Applied Physics*. 2013;46(40):404001.

21. Luz AR, Santos LS, Lepienski CM, Kuroda PB, Kuromoto NK. Characterization of the morphology, structure and wettability of phase dependent lamellar and nanotube oxides on anodized Ti-10Nb alloy. *Applied Surface Science*. 2018;448:30-40.

22. Klapkiv MD, Povstyana NY, Nykyforchyn HM. Production of conversion oxide-ceramic coatings on zirconium and titanium alloys. *Materials Science*. 2006;42(2):277-286.

23. Wang R, He X, Gao Y, Zhang X, Yao X, Tang B. Antimicrobial property, cytocompatibility and corrosion resistance of Zn-doped ZrO_2/TiO_2 coatings on Ti6Al4V implants. *Materials Science and Engineering: C*. 2017;75:7-15.

24. Choi JW, Kim GW, Shin KR, Yoo B, Shin DH. Synthesis of Zirconium-Titanium oxide mixed layers on Ti substrates by plasma electrolytic oxidation and plasma-enhanced. *Journal of Alloys and Compounds*. 2017;726:930-938.

25. Cueto LF, Sánchez E, Torres-Martínez LM, Hirata GA. On the optical, structural, and morphological properties of ZrO_2 and TiO_2 dip-coated thin films supported on glass substrates. *Materials Characterization*. 2005;55(4-5):263-271.

26. Baltrusaitis J, Mendoza-Sanchez B, Fernandez V, Veenstra R, Dukstiene N, Roberts A, et al. Generalized molybdenum oxide surface chemical state XPS determination via informed amorphous sample model. *Applied Surface Science*. 2015;326:151-161.

27. Hanawa T, Ota M. Characterization of surface film formed on titanium in electrolyte using XPS. *Applied Surface Scienc*e. 1992;55(4):269-276.

28. Hanawa T, Ota M. Calcium phosphate naturally formed on titanium in electrolyte solution. *Biomaterials*. 1991;12(8):767-774.

29. Sasahara A, Murakami T, Tomitori M. XPS and STM study of TiO_2(110)-(1x1) surfaces immersed in simulated body fluid. *Surface Science*. 2018;668:61-67.

30. Moulder JF, Chastain J, ed. *Handbook of X-ray Photoelectron Spectroscopy: A Reference Book of Standard Spectra for Identification and Interpretation of XPS Data*. Waltham: Physical Electronics Division, Perkin-Elmer Corporation; 1992.